



Trans. Nonferrous Met. Soc. China 32(2022) 2935-2947

Transactions of Nonferrous Metals Society of China

www.tnmsc.cn



# Microstructures and interfacial interactions of Al<sub>2</sub>O<sub>3</sub> whiskers and graphene nano-platelets co-reinforced copper matrix composites

Zhen-yi SHAO<sup>1,2</sup>, Heng-kang PAN<sup>2</sup>, Rui SHU<sup>3</sup>, Xiao-song JIANG<sup>1</sup>, Min-hao ZHU<sup>1</sup>

- 1. School of Materials Science and Engineering, Southwest Jiaotong University, Chengdu 610031, China;
- 2. School of Materials and Environmental Engineering, Chengdu Technological University, Chengdu 611730, China;
  - 3. Forschungszentrum Jülich GmbH, Institut für Energie-und Klimaforschung-Plasmaphysik, 52425 Jülich, Germany

Received 27 September 2021; accepted 2 March 2022

**Abstract:** The mechanical properties and microstructures of Al<sub>2</sub>O<sub>3</sub> whiskers and graphene nano-platelets (GNPs) co-reinforced Cu-matrix composites were studied. Cu-matrix composites with a variation of GNPs amount were fabricated by mechanical alloying followed by vacuum hot-pressing sintering and hot isostatic pressing. The Cu-matrix composite with 0.5 wt.% GNPs (GNPs-0.5) suggests a good interfacial bonding of both Cu/C and Cu/Al<sub>2</sub>O<sub>3</sub> interfaces. Both the hardness and compressive strength of Cu-matrix composites show a consistent tendency that firstly increases to a critical value and then decreases with increasing GNPs amount. It is suggested that the most possible strengthening mechanisms of both GNPs and Al<sub>2</sub>O<sub>3</sub> whisker working in the Cu-matrix composites involve energy dissipating and load transfer, as well as grain refinements for GNPs. The synergetic effect of GNPs and Al<sub>2</sub>O<sub>3</sub> whiskers is highlighted that the embedded GNPs would hinder the crack path generated at the Al<sub>2</sub>O<sub>3</sub>/Cu interface and enhance the already outstanding strengthening effect that Al<sub>2</sub>O<sub>3</sub> whiskers provide.

Key words: graphene; Al<sub>2</sub>O<sub>3</sub> whisker; Cu-matrix composite; microstructure; interfacial interaction

### 1 Introduction

Copper-matrix composites have been widely investigated by researchers for applications in electronic packaging, heat sinks, and friction materials owing to their excellent mechanical properties, good electrical conductivities, and excellent wear and corrosion resistances [1]. Reinforcements impart special properties to the composite and are often used to tailor the properties of composites to meet special requirements. For instance, high volume TiC particles can improve hardness, strength and wear resistance of Cu-matrix composites, but reduce their ductility and fracture toughness [2]. Owing to the limited strengthening effect of single-phase

reinforcements [3], multiphase reinforcements, with synergetic strengthening and toughening effects of different reinforcements, have attracted significant attention in recent years [4,5]. Al-Cu composites with biphasic reinforcements of SiC and MoS<sub>2</sub> [6] have been reported to exhibit improved microhardness, corrosion resistance, and wear resistance. In Cu-matrix composites co-reinforced with carbon nanotubes (CNTs) and TiB2 microparticles [7], the TiB<sub>2</sub> microparticles improve the homogeneous dispersion of CNTs and promote thermal mismatch and load transfer mechanisms, demonstrating the synergistic strengthening effect of nano- and microreinforcements. Similarly, in Al-matrix composites co-reinforced with CNTs and SiC particles [8], SiC particles inhibit the pull-out of CNTs and achieve synergistic strengthening via the pinning effect.

Alumina (Al<sub>2</sub>O<sub>3</sub>) whiskers have superior heat and chemical stabilities, high strength and elasticity modulus, and excellent wear and oxidation resistances [9]. Al<sub>2</sub>O<sub>3</sub> whiskers are preferred over (carbides non-oxide secondary phases carbonaceous materials) for high-temperature structural applications, such as engine pistons and brake disks. This is because non-oxide phases undergo oxidation, and their mechanical properties deteriorate at elevated temperatures in the atmosphere [9-12]. CORROCHANO et al [13] reported that Al<sub>2</sub>O<sub>3</sub> whiskers have more noteworthy effect on the mechanical properties of Al-matrix composite than Al<sub>2</sub>O<sub>3</sub> particles because of better interfacial bonding. IQBAL et al [14] researched the fatigue crack growth mechanism of cast Al-matrix composites co-reinforced with SiC particles and Al<sub>2</sub>O<sub>3</sub> whiskers and reported that these composites exhibit a higher threshold stress intensity factor range ( $\Delta K_{\text{th}}$ ) and better resistance to crack growth than those co-reinforced with Al<sub>2</sub>O<sub>3</sub> whiskers and cast Al alloy. Graphene, constituting a two-dimensional (2D) hexagonal lattice of carbon atoms [15], has been widely researched as a reinforcement phase for polymers [16], ceramics [17], and metals [3,18] owing to its extraordinary mechanical properties [19] originating from the sp<sup>2</sup> hybridisation of carbon excellent electrical atoms, and thermal conductivities [20], self-lubricating properties, and good wear resistance [21]. Graphene has a unique planar 2D structure with a large specific surface area, which provides more area to interact with the matrix material than the tubular one-dimensional (1D) structure of CNTs [19,20]. GÜLER and BAGCI [22] reviewed the mechanical properties of graphene reinforced metal matrix composites and reported that apart from the graphene content, other factors, such as distribution, orientation, and production type of graphene also affect the mechanical properties of the composites. MOGHADAM et al [21] reviewed the mechanical and tribological properties of self-lubricating metal matrix nanocomposites reinforced with CNTs and graphene. They reported that a uniform distribution of graphene and CNTs in the metal matrix makes the nanocomposites achieve favourable properties such as high strength and self-lubrication.

 $\label{eq:continuous} Even \ though \ Al_2O_3 \ whiskers \ or \ graphene$  have been widely researched as single-phase

reinforcements in metal matrix composites, their synergetic effects on the mechanical properties and strengthening mechanisms of Cu-matrix composites have rarely been reported. Because of the flexibility of graphene and the rigidity of Al<sub>2</sub>O<sub>3</sub> whiskers, it would be interesting to analyse the interaction between graphene and Al<sub>2</sub>O<sub>3</sub> whiskers for any additional advantages besides their individual strengthening effects. Therefore, in the present study, Al<sub>2</sub>O<sub>3</sub> whiskers (1D) and graphene (2D) were used as reinforcements, and their interfacial interactions and hybrid strengthening mechanisms were analysed. The Cu-matrix composites with reinforcements fabricated biphasic were mechanical alloying followed by vacuum hot-pressing sintering (HP) and hot isostatic pressing (HIP) [20,23,24]. The effects of graphene content on the mechanical properties and microstructures of the Cu-matrix composites were studied. In addition, the Cu/C and Cu/Al<sub>2</sub>O<sub>3</sub> interfacial bonding states and biphasic hybrid strengthening mechanisms were analysed in detail.

### 2 Experimental

### 2.1 Raw materials and surface treatment

Graphene nano-platelets (GNPs) (5-10 layers, purity  $\geq 99\%$ , and density of 2.1 g/cm<sup>3</sup>) and Al<sub>2</sub>O<sub>3</sub> whiskers (purity  $\geq 99\%$ , and density of 3.99 g/cm<sup>3</sup>) were purchased from Shanghai Naiou Nano Technology Co., Ltd. (China). The chemical reagents used in this work were purchased from Chengdu Kelong (China). To improve the dispersion uniformity in the Cu matrix and the surface wettability with Cu atoms, the GNPs and Al<sub>2</sub>O<sub>3</sub> whiskers were surface-functionalised in Rutin deionised water solution (0.02 µg/mL) and lauryl sodium sulphate deionised water solution (2 g/L)along with ultrasonic dispersion, respectively, followed by suction filtration and drying. Electrolytic Cu powder (<74 μm, purity  $\geq$ 99.9%, and density of 8.9 g/cm<sup>3</sup>) was used as the matrix.

### 2.2 Fabrication of bulk composites

Bulk Cu-matrix composites were fabricated by mechanical alloying, vacuum hot-pressing sintering, and hot isostatic pressing, consecutively, as illustrated in Fig. 1. By adjusting the content of GNPs, a series of Cu-matrix composite powders containing 1.0 wt.% Al<sub>2</sub>O<sub>3</sub> whiskers and 0, 0.25, 0.5, and 1.0 wt.% GNPs were synthesised. The composite powders were ball-milled for 2 h at a rotational speed of 350 r/min in a planetary ball mill (WL-1). The ball-to-powder ratio was 4:1, and tertiary butanol was used as the milling medium. The ball-milled powders were dried in a freezedrying oven (FD-A-50). Then, the composite powders were sintered into discs with diameter of 60 mm by vacuum hot-pressing sintering at 900 °C and 14 MPa for 2 h. Subsequently, the composites were re-sintered into discs (60 mm in diameter) by hot isostatic pressing at 900 °C and 100 MPa for 2 h. The bulk Cu-matrix composites with 0, 0.25, 0.5, and 1.0 wt.% GNPs are denoted as GNPs-0, GNPs-0.25, GNPs-0.5, and GNPs-1.0, respectively. A Cu-matrix composite without Al<sub>2</sub>O<sub>3</sub> and 0.5 wt.% GNPs was also synthesised, which is denoted as  $Al_2O_3-0.$ 

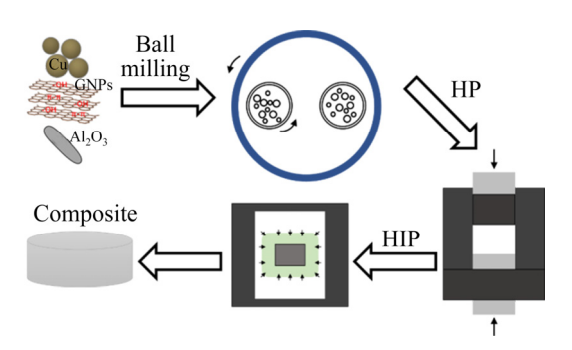


Fig. 1 Schematic diagram of composite fabrication

### 2.3 Characterizations

X-ray diffraction (TD-3500) was employed to analyse the phase compositions of the composite powders and bulk composites. The microstructures of the ball-milled composite powders and bulk composites were examined using scanning electron microscopy (JEOL JSM-7001F) with Bruker X-ray energy dispersive spectrometer (EDS). Transmission electron microscopy (FEI Tecnai F20ST) was used to characterise the microstructures of the bulk composites. The density of the bulk composites was measured using an AR-150 ME density tester based on Archimedes drainage method. The Vickers hardness values of the bulk composites were obtained using a micro-hardness tester (HXD-100TM/LCD). Compression and shear tests of the composites were performed on a WDW-3100 universal testing machine.

### 3 Results and discussion

### 3.1 Microstructures of composite powders and bulk composites

Figure 2 displays the microstructural features of ball-milled composite powders and sintered bulk composites. Cu particles with different morphologies and sizes are observed, some maintaining the originally spherical shape and size but some deforming into large particles with irregular shape. The deformation is caused by repeated cycles of cold welding among particles, large particle rupture and repeated welding of metallic particles during ball milling [15]. Besides surface functionalisation of GNPs and Al<sub>2</sub>O<sub>3</sub> whiskers, ball milling can regulate the dispersions of these reinforcements in the Cu matrix. Figures 2(b, d) show that uniformly distributed GNPs with morphological integrity are unfolded and overlap the Cu atoms. During the process of ball milling, the large specific surface can provide sufficient contact area between GNPs and Cu particles, and the collision between GNPs and Cu particles can effectively improve interfacial bond strength at the Cu/C interface [3]. Al<sub>2</sub>O<sub>3</sub> whiskers with diameters of 1-2 µm and lengths up to several tens of micrometres are uniformly distributed in the Cu matrix. Figures 2(e, f) show the surface morphology of the bulk GNPs-0.5 composite; graphene and Al<sub>2</sub>O<sub>3</sub> whiskers are randomly embedded in the Cu matrix, as indicated by Spots 4 and 5, respectively. No significant porosity is observed on the surface, and no distinct cracks are observed at Cu/C or Cu/Al<sub>2</sub>O<sub>3</sub> interfaces. This indicates that the sintered bulk Cu-matrix composites exhibit relatively high density and favourable interfacial bonding, as confirmed using additional characterisation techniques.

The XRD patterns of the ball-milled composite powders and sintered bulk Cu-matrix composites are shown in Fig. 3. All the composite powders show identical diffraction peaks at  $2\theta$ =42.3°, 50.4°, 74.1°, 89.9° and 95.1°, corresponding to (111), (200), (220), (311), and (222) planes of Cu, respectively (JCPDS Card No. 04-0836). No peaks corresponding to graphene or Al<sub>2</sub>O<sub>3</sub> are observed, probably because of their low amounts and random distributions. The diffraction patterns of the sintered bulk composites are similar to those of composite

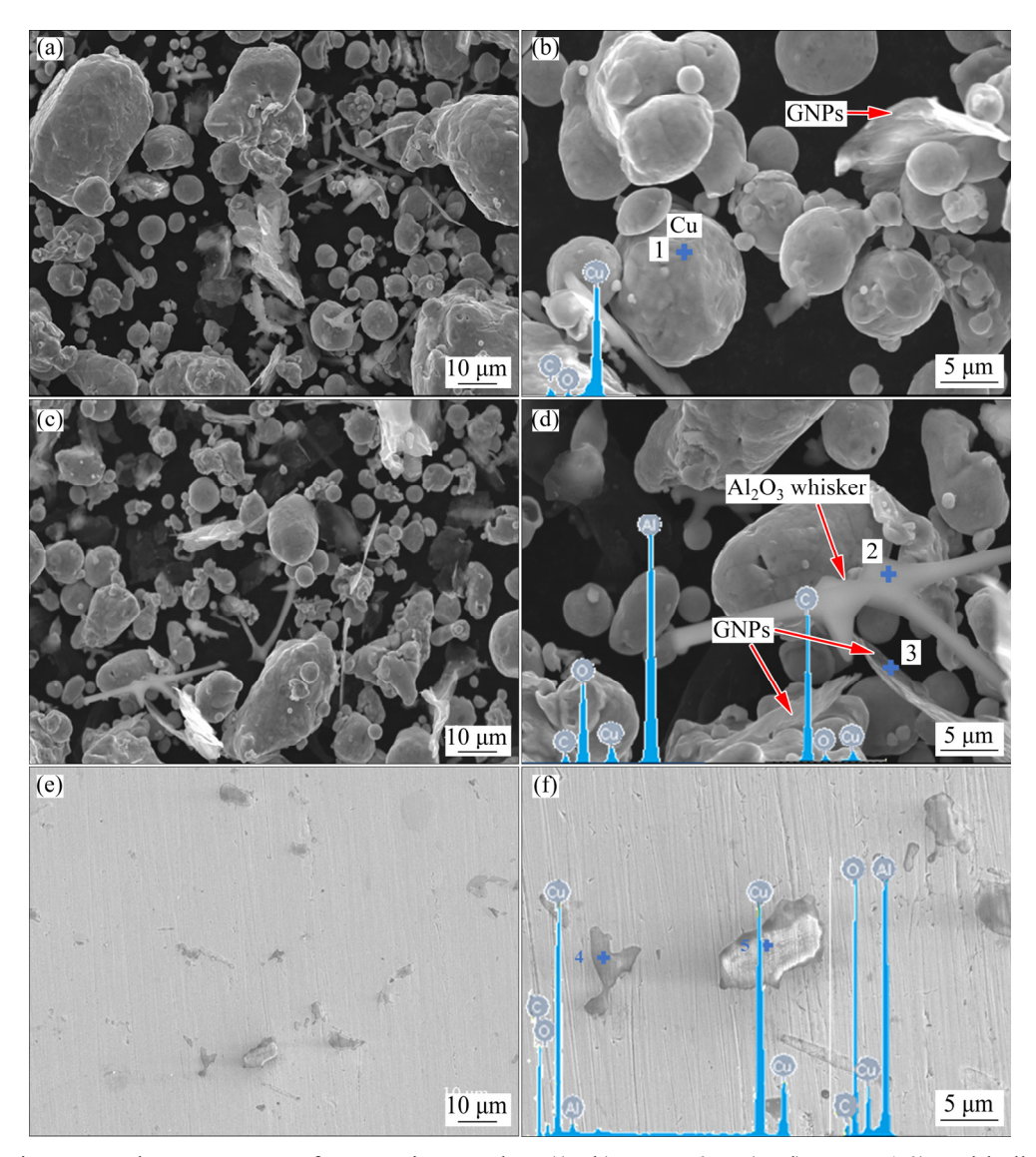


Fig. 2 SEM images and EDS spectra of composite powders ((a, b) GNPs-0.5; (c, d) GNPs-1.0) and bulk composites ((e, f) GNPs-0.5)

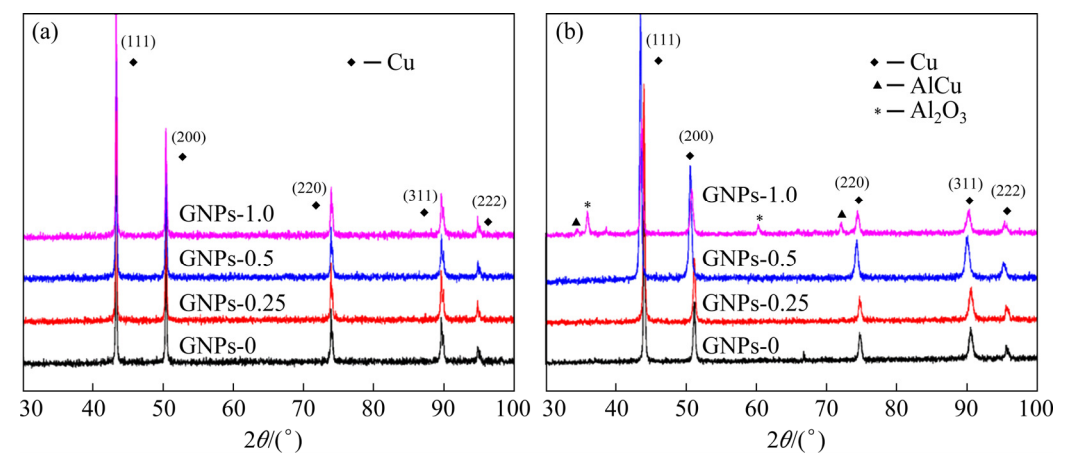


Fig. 3 XRD patterns of ball-milled composite powders (a) and sintered bulk Cu matrix composites (b)

powders, except for the appearance of new peaks in the pattern of GNPs-1.0. The diffraction peaks

located at approximately  $2\theta$ =35.7° and 60.1° correspond to aluminium oxide (JCPDS Card Nos.

51-0769 and 46-1131). The diffraction peaks located at approximately  $2\theta$ =34.4° and 72.0° correspond to cupalite (AlCu) and aluminium copper (AlCu), respectively (JCPDS Card Nos. 39-1371 and 26-0016). The origin of these peaks is attributed to the interfacial interaction between the Cu matrix and Al<sub>2</sub>O<sub>3</sub> whiskers. Since Al<sub>2</sub>O<sub>3</sub> whiskers are uniformly distributed in the Cu matrix and their amounts are identical in each composite, the random presence of Al<sub>2</sub>O<sub>3</sub>-related diffraction peaks may be related to the preparation of the tested specimens.

Figure 4 shows the TEM images and the corresponding selected area electron diffraction (SAED) patterns of GNPs-0.5 composite. The morphologies of the Cu matrix and the surrounding biphasic reinforcements of GNPs and Al<sub>2</sub>O<sub>3</sub> whiskers are evident in Fig. 4(a). The EDS results (obtained from the spot marked by a red cross in Fig. 4(a)) and the SAED pattern in Fig. 4(b) indicate the presence of graphene. The wrinkled

GNPs embedded in the Cu matrix has a clear and strong bonding interface with the Cu matrix (Fig. 4(b)). The high-resolution TEM (HRTEM) image in Fig. 4(d) shows a transition layer of several nanometres thickness between the Cu matrix and GNPs. In addition, no microvoids are observed along the interface, suggesting good interfacial bonding. Figure 4(c) shows the presence of Al<sub>2</sub>O<sub>3</sub> whiskers (EDS results) and a direct bonding interface between the Cu matrix and Al<sub>2</sub>O<sub>3</sub> whiskers. To further investigate the interfacial bonding state between the Cu matrix and Al<sub>2</sub>O<sub>3</sub> whiskers, bright-field TEM and SAED studies were carried out, and the results are shown in Fig. 5. The EDS results from the spot marked by a red cross in Fig. 5(a) reveal the presence of Al<sub>2</sub>O<sub>3</sub> whiskers, and the SAED pattern (Fig. 5(c)) of the whisker along the zone axis of [010] corresponds to a single crystal of hexagonal  $\alpha$ -Al<sub>2</sub>O<sub>3</sub> [9]. The HRTEM image in Fig. 5(d) reveals a periodic lattice structure and two sets of fringes with d-spaces of

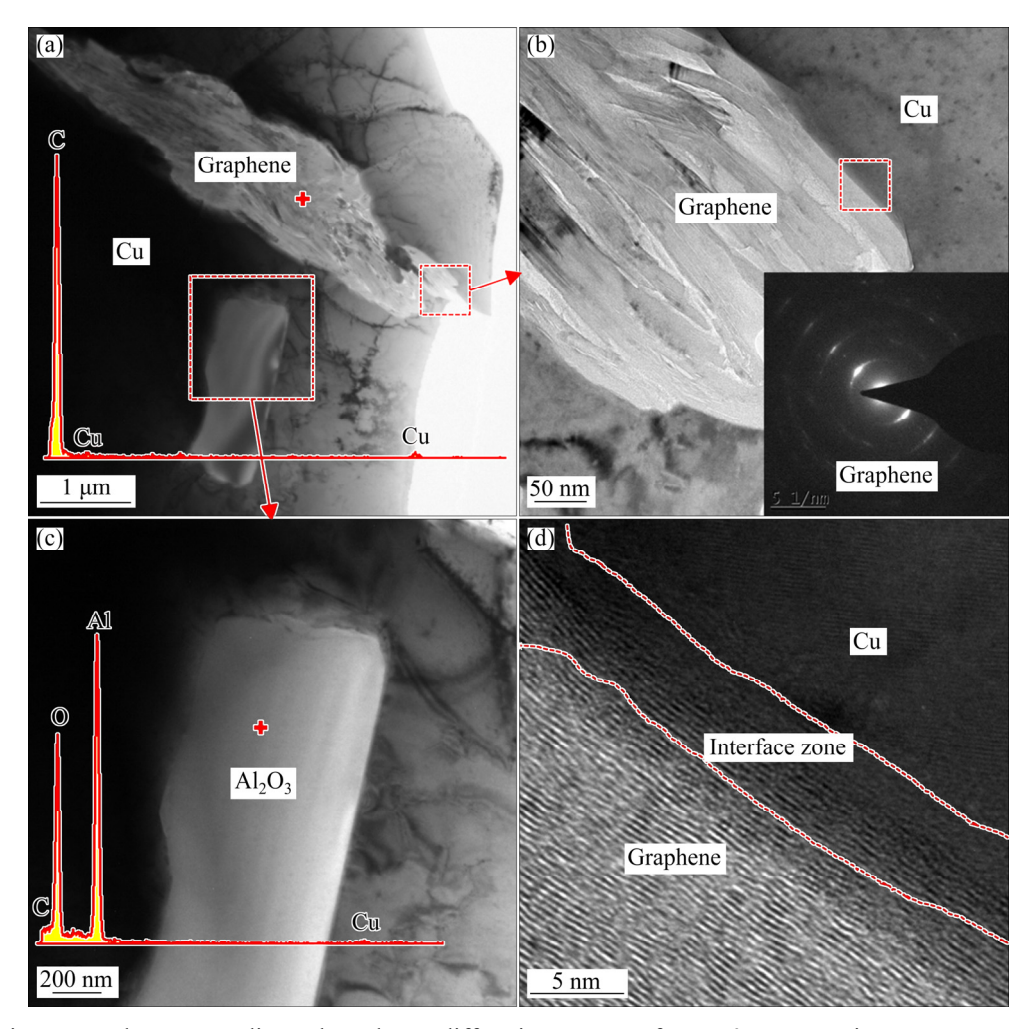


Fig. 4 TEM images and corresponding selected area diffraction pattern of GNP-0.5 composite

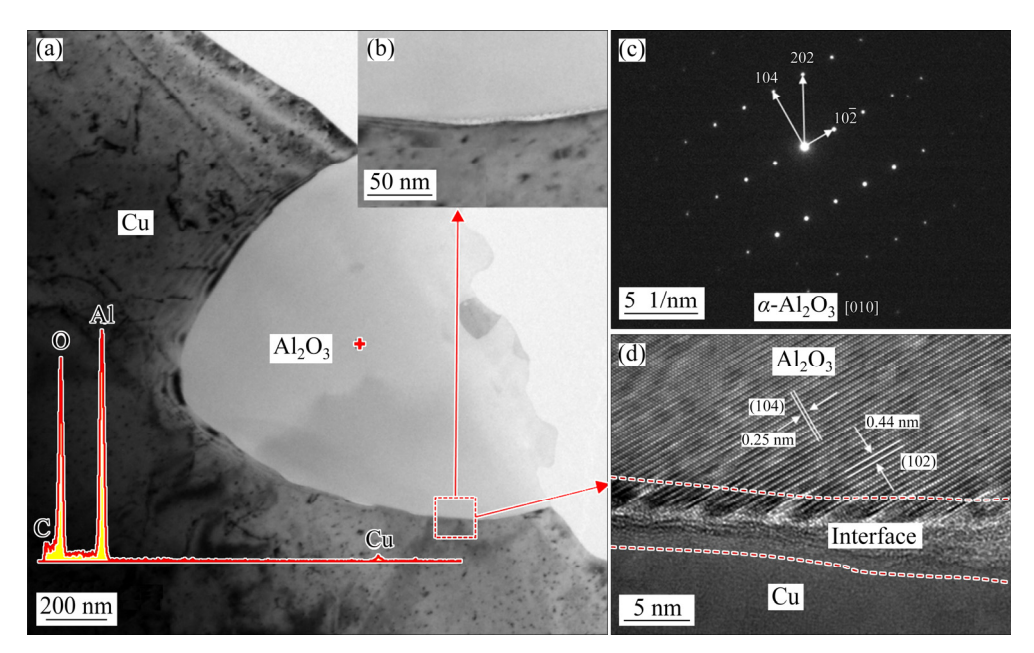


Fig. 5 TEM images of Cu/Al<sub>2</sub>O<sub>3</sub> interface and corresponding selected area diffraction pattern of GNP-0.5 composite

0.25 and 0.44 nm corresponding to the (104) and (102) planes of  $\alpha$ -Al<sub>2</sub>O<sub>3</sub>, respectively (JCPDS Card Nos. 10-0173 and 10-0414). The HRTEM image in Fig. 5(d) displays a transition layer of several nanometres thickness between the Cu matrix and  $\alpha$ -Al<sub>2</sub>O<sub>3</sub>, which may be attributed to the interfacial interaction between Cu and  $\alpha$ -Al<sub>2</sub>O<sub>3</sub>, i.e., diffusion of Cu into the  $\alpha$ -Al<sub>2</sub>O<sub>3</sub> lattice. Overall, the microstructural characteristics of GNPs-0.5 composite suggest good interfacial bonding at Cu/C and Cu/Al<sub>2</sub>O<sub>3</sub> interfaces, which is crucial to enhancing the mechanical properties of composites.

#### 3.2 Mechanical properties

The relative density, Vickers hardness, compressive strength, and shear strength were determined to investigate the effect of GNPs content on the mechanical properties of the bulk Cu-matrix composites. The results are listed in Table 1 and illustrated in Fig. 6. The relative densities of all Cu-matrix composites are >98.5% with no significant differences, indicating that all the bulk composites are densified by the consecutive application of mechanical alloying, vacuum hot-pressing sintering, and hot isostatic pressing. The Vickers hardness of the Cu-matrix composite co-reinforced with GNPs and Al<sub>2</sub>O<sub>3</sub> whiskers is higher than that of single phase (GNPs or Al<sub>2</sub>O<sub>3</sub> whiskers) reinforced Cu-matrix composites (HV 47.9 and 58.6, respectively). The

**Table 1** Mechanical properties of bulk Cu matrix composites

Specimen	Relative density/ %	Hardness (HV)	Compressive strength/ MPa	Shear strength/ MPa
Al <sub>2</sub> O <sub>3</sub> -0	98.5	47.9±4.3	_	123.7±3.6
GNPs-0	99.4	58.6±2.3	$141.9 \pm 11.8$	$163.3 \pm 1.7$
GNPs-0.25	98.9	62.6±1.9	151.4±10.5	$143.2 \pm 2.3$
GNPs-0.5	99.3	84.9±3.8	221.2±8.4	133.7±1.1
GNPs-1.0	99.1	74.6±3.0	195.3±7.2	120.1±2.4

hardness of the composites increases from HV 58.6 to 84.9 with the presence of both GNPs and Al<sub>2</sub>O<sub>3</sub> whiskers. GNPs-0.5 exhibits a significantly higher hardness than the other composites, e.g., its hardness is 44.9% higher than that of GNPs-0. The addition of GNPs in the Cu matrix enhances the compressive strength of Cu composites from 141.9 to 221.2 MPa. Consistent with the hardness, GNPs-0.5 has a significantly higher compressive strength than the other composites, approximately 55.9% higher than that of GNPs-0. The hardness and compressive strength of Cu-matrix composites show the same trend: first increases to a critical value and then decreases with increase in the content of GNPs. The shear strength of the Cu-matrix composites co-reinforced with GNPs and Al<sub>2</sub>O<sub>3</sub> whiskers is higher than that of GNPsreinforced Cu composites (123.7 MPa). However, with increase in the content of GNPs, the shear strength of the Cu-matrix composites monotonously reduces from 163.3 to 120.1 MPa. The shear fractography was examined to analyse the decrease in the shear strength, and the results are shown in Fig. 7. The fracture surface of GNPs-0 composite (Fig. 7(a)) shows elongated dimples and Al<sub>2</sub>O<sub>3</sub> whiskers parallel to the fracture surface. This indicates that GNPs-0 undergoes moderate amount

of plastic deformation; however, no obvious cracks are observed on the fracture surface. In contrast, the fracture surface of GNPs-0.5 composite (Fig. 7(b)) shows no apparent dimple and tear ridge structure, indicating slight plastic deformation. In addition, a large amount of microcracks and microvoids are observed, which are typical of brittle fracture.

The increases in the hardness and compressive strength are attributed to the strengthening effects

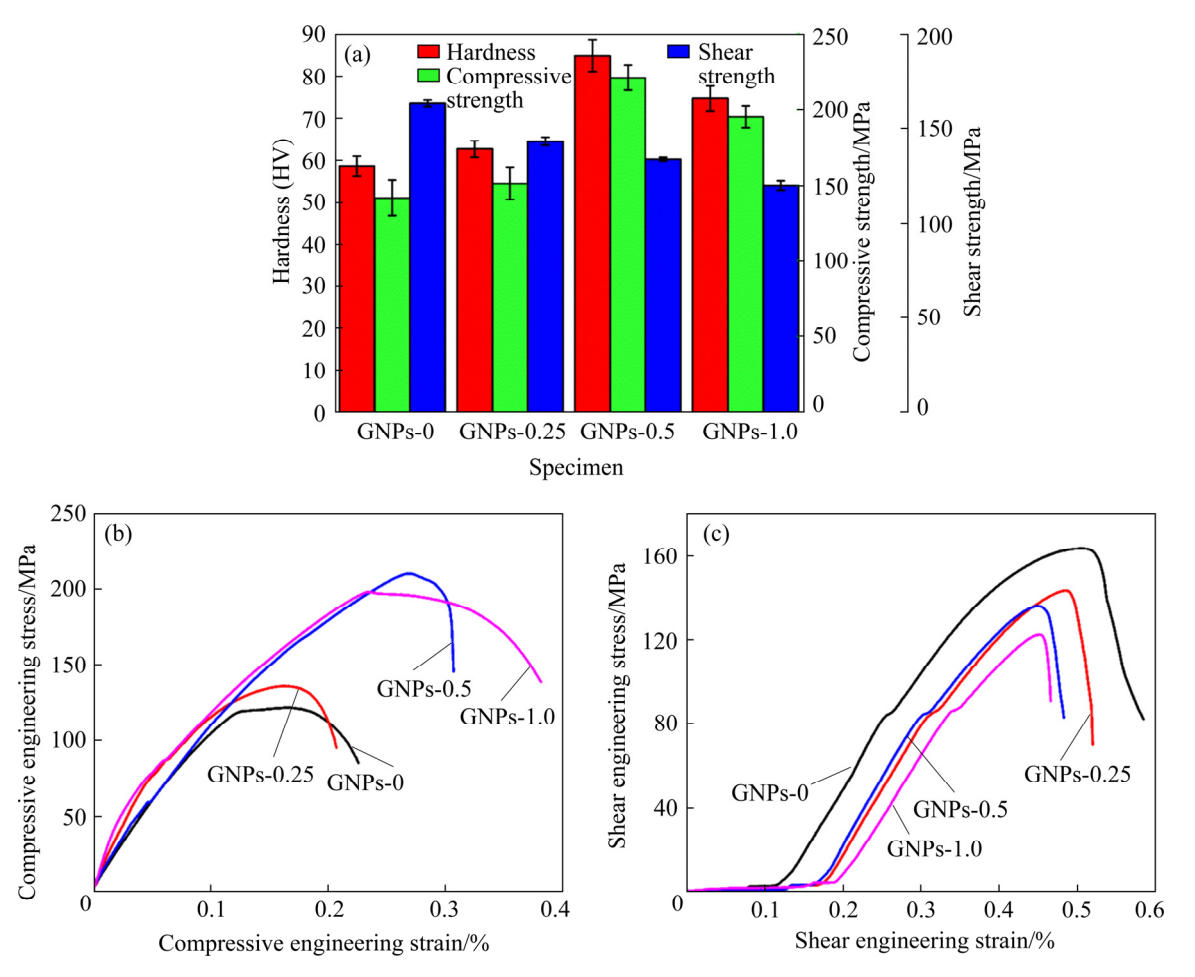


Fig. 6 Mechanical properties and engineering stress-strain curves of bulk Cu matrix composites: (a) Vickers hardness, compressive strength and shear strength; (b) Compressive engineering stress-strain curves; (c) Shear engineering stress-strain curves

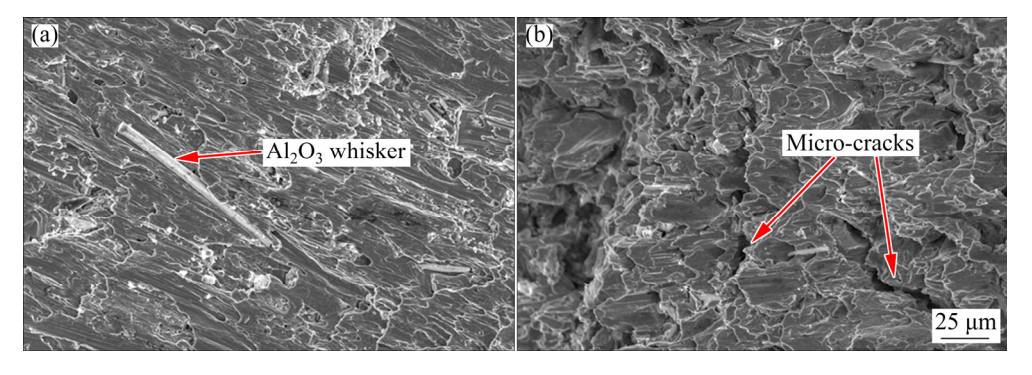


Fig. 7 SEM images of shear fractures of bulk Cu matrix composites: (a) GNP-0; (b) GNP-0.5

of Al<sub>2</sub>O<sub>3</sub> whiskers and well-dispersed GNPs originating from their outstanding mechanical properties and good interfacial bonding with the Cu matrix, wherein GNPs play a primary role. However, when the amount of GNPs is further increased to 1.0%, agglomeration of GNPs is inevitable, which causes defects and subsequent deterioration of hardness and compressive strength. As discussed above, the interfacial bonds of Cu/C and Cu/Al<sub>2</sub>O<sub>3</sub> are strong; however, some weak bonding still exists. The compressive stress can reduce the weak bonding at interfaces as a large contacting area between GNPs and Cu matrix and accordingly counteract the effects caused by weak bonding, such as debonding or separation, at the interface. Nonetheless, an adverse effect is obtained when the composites are exposed to a shear stress, which can intensify the effects caused by weak bonding. On the one hand, the poorly bonded interfacial areas may separate or debond and generate microvoids at the interface, which act as a source of microcracks. On the other hand, increased amount of GNPs may agglomerate and form defects in the Cu matrix, resulting in stress concentration and generation of microcracks. The generated microcracks propagate along the interface under an external shear force, leading to the deterioration of shear strength of composites [1,12].

## 3.3 Interfacial interactions and strengthening mechanisms

GNPs can affect the sintering behaviour and microstructure of composites. NIETO et al [25] reported that the grain growth was restrained by the introduction of GNPs in a ceramic matrix. The grain refinement was strongly depended on the contact state or wrapping of matrix grains. As shown in Fig. 8, the Cu grains (marked by red arrows) are wrapped or trapped by the GNPs to form fine grains, indicating that GNPs inhibit grain growth during sintering. The wrapping or trapping of GNPs is a mechanism that occurs during sintering and contributes to the grain refinement of Cu-matrix composites [20,26]. However, the increased suppression of grain growth caused by wrapping of Cu grains by GNPs (at higher amounts) adversely affects the densification of Cu-matrix composites [20].

To better understand the strengthening effects of GNPs in Cu composites, SEM images of the

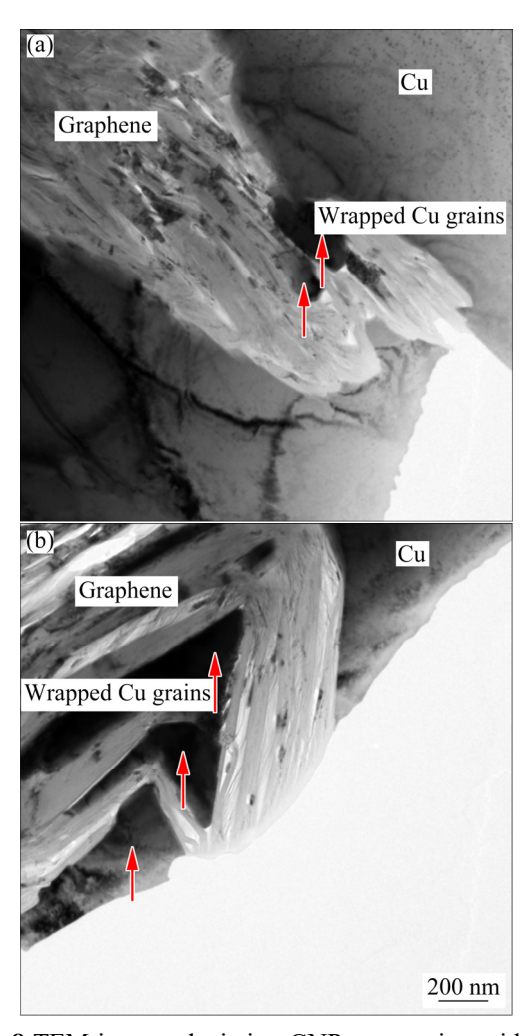


Fig. 8 TEM images depicting GNPs contacting with and wrapping around Cu grains in GNP-0.5 composite

fractured specimens were obtained, as shown in Fig. 9. The cracked area shows the presence of pulled-out GNPs (Fig. 9(a)), and the exposed GNPs stride over the crack and act as a bridge to connect the separated matrix (Fig. 9(b)). Both these processes are accompanied by deformation of the GNPs, such as bending or kinking. Once the Cu matrix is fractured, GNPs deform to consume the strain energy and subsequently pull out and bridge over the separated matrix, resulting in energy dissipation and improvement in the fracture strength [19]. A good interfacial bonding between GNPs and Cu as illustrated in Fig. 4(d) can effectively transfer the load and avoid stress concentration, which plays a vital role as an extrinsic strengthening mechanism [22]. When GNPs interact with the surrounding Cu matrix, extrinsic strengthening or toughening mechanisms are involved, such as solution strengthening of

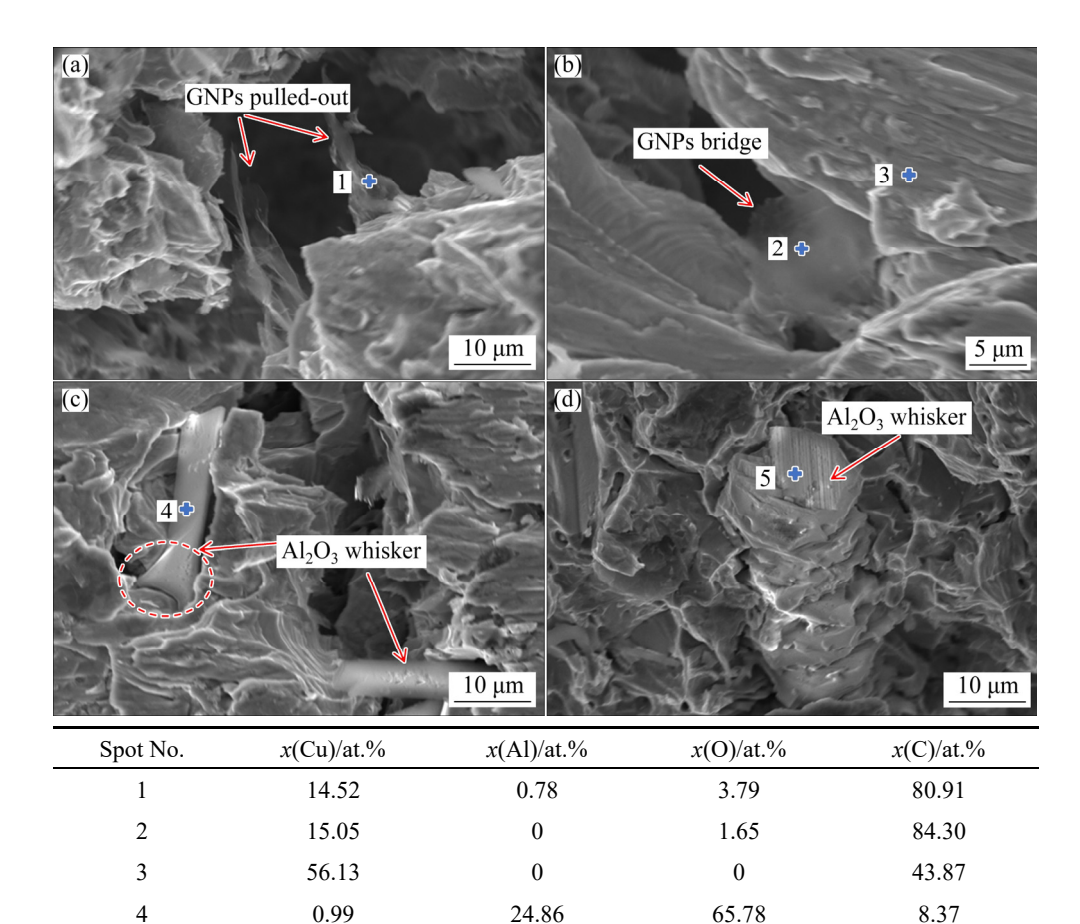


Fig. 9 Failure behaviors of graphene and  $Al_2O_3$  whiskers in Cu matrix composites and EDS results for corresponding spots: (a) Graphene pulled-out in GNP-1.0 composite; (b) Graphene bridge in GNP-1.0 composite; (c)  $Al_2O_3$  deformation in GNP-0.5 composite; (d)  $Al_2O_3$  cleavage fracture in GNP-0.5 composite

27.53

62.45

carbon atoms [27], Orowan strengthening, and dislocation strengthening due to thermal mismatch between the GNPs and the matrix [20]. As the solubility of C in a Cu matrix is extremely low, the solution strengthening of C atoms in the Cu matrix is limited. Effective Orowan looping usually occurs in composites with GNPs uniformly distributing inside the grains rather than at the grain boundaries [28]. Considering the large specific surface area and structural integrity of GNPs, Orowan strengthening can also be ignored. The thermal mismatch between GNPs and the Cu matrix is also not effective according to the microstructure of the Cu/C interface. Therefore, grain refinement by wrapping or trapping of GNPs (Fig. 10(a)), energy dissipation in the form of deformation and subsequent pulling-out or bridging of GNPs (Fig. 10(b)), and effective load transfer (Fig. 10(c)) are considered as the most possible strengthening mechanisms of GNPs in the Cu-matrix composites.

5

0.46

The strengthening behaviour of the Al<sub>2</sub>O<sub>3</sub>

whiskers in the Cu-matrix composites is shown in Fig. 9. It is evident that the Al<sub>2</sub>O<sub>3</sub> whiskers deform under shear stress to dissipate energy (Fig. 9(c)), and the pulled-out Al<sub>2</sub>O<sub>3</sub> whiskers act as a bridge to connect the separated matrix, similar to the bridging behaviour of GNPs. A possibility that the Al<sub>2</sub>O<sub>3</sub> whiskers are debonded from the Cu matrix because of their coarse outer surface is shown in Fig. 9(d). This may be attributed to the interface debonding at the transition layer between Al<sub>2</sub>O<sub>3</sub> and Cu matrix as discussed above. Another possibility is the loss of integrity of Al<sub>2</sub>O<sub>3</sub> whiskers during the fabrication processes. Al<sub>2</sub>O<sub>3</sub> whiskers exhibit cleavage fracture under external load, dissipating energy and strengthening the matrix. It has been reported that the primary reason for microcrack generation composites reinforced with discontinuous particulates or whiskers is debonding or separation at the interface between the reinforcement and the matrix [12,29]. Figure 11(b) shows the interfacial bonding state of Al<sub>2</sub>O<sub>3</sub>/Cu as the crack initiates and

9.56

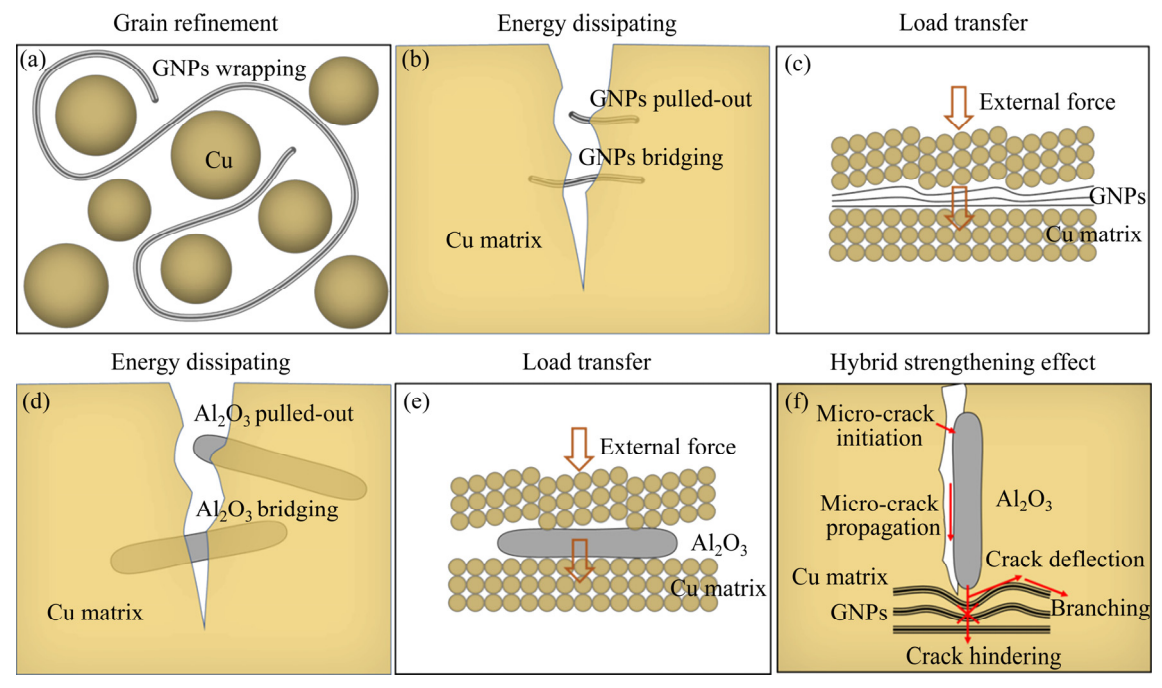


Fig. 10 Strengthening mechanisms of GNPs (a, b, c), Al<sub>2</sub>O<sub>3</sub> whiskers (d, e), and hybrid effect (f) in Cu composites

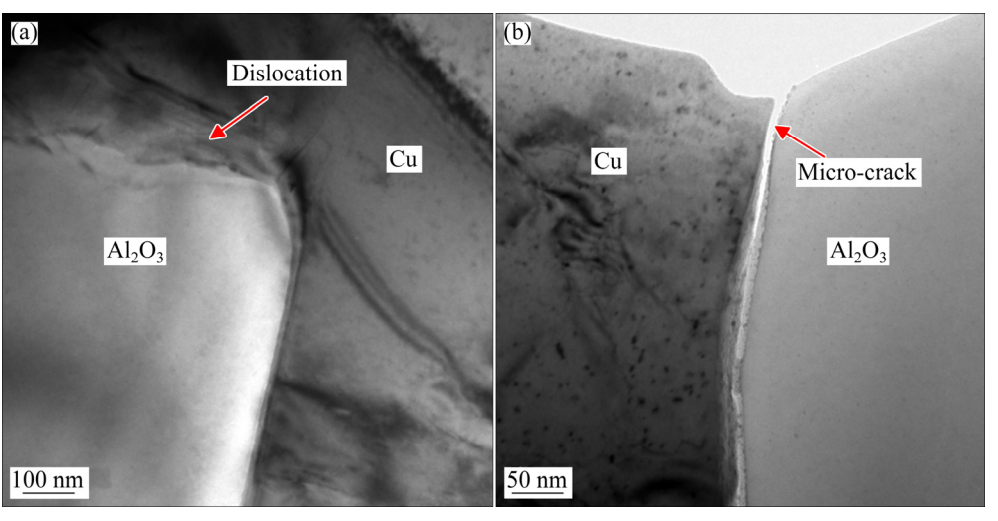


Fig. 11 TEM images depicting dislocation (a) and debonding at Al<sub>2</sub>O<sub>3</sub>/Cu interface (b) in GNP-0.5 composite

then propagates through Al<sub>2</sub>O<sub>3</sub> and Cu interfaces. Because the stiffness of Al<sub>2</sub>O<sub>3</sub> whiskers is much higher than that of Cu, they do not undergo plastic transformation under external load; therefore, the stress on the Al<sub>2</sub>O<sub>3</sub>/Cu matrix interface increases, and the edges of the stiff Al<sub>2</sub>O<sub>3</sub> whiskers act as a stress concentrator. Furthermore, strain mismatch accumulates, and the dislocation density of the Cu matrix increases near the interface, as shown in Fig. 11(a). Furthermore, when the stress on the Al<sub>2</sub>O<sub>3</sub>/Cu matrix interface arising from the large strain mismatch increases and exceeds the interfacial bonding strength, interface debonding occurs and results in crack initiation [12]. The

Al<sub>2</sub>O<sub>3</sub> whiskers in the Cu matrix promote energy dissipation (Fig. 10(d)) and load transfer (Fig. 10(e)) because of their high strength, hardness, and modulus. Moreover, dislocation strengthening due to the strain mismatch and different coefficients of thermal expansion between Al<sub>2</sub>O<sub>3</sub> and Cu-matrix is also a significant strengthening mechanism [1,20].

Evidently, the synergetic strengthening effects of GNPs and Al<sub>2</sub>O<sub>3</sub> whiskers enhance the mechanical properties of Cu-matrix composite. Nonetheless, the interfacial interaction at C/Al<sub>2</sub>O<sub>3</sub> interface and the fracture mechanism of Cu matrix co-reinforced with GNPs and Al<sub>2</sub>O<sub>3</sub> whiskers are still not completely understood, and very few

related studies have been reported. In an Al-alloy matrix co-reinforced with Al<sub>2</sub>O<sub>3</sub> whiskers and SiC particles [12], the interaction between Al<sub>2</sub>O<sub>3</sub> whiskers and SiC particles provided synergetic strengthening effects, resulting in a high stress at the interfaces, less interfacial debonding, and high fatigue strength of the composite. Furthermore, it has been extensively reported that graphene nanosheets uniformly dispersing in a matrix can block the dislocation motion and strengthen the mechanical properties of composites [30,31]. Graphene interfaces in nanolayered composites can also hinder crack propagation [32]. Furthermore, the crack path changes because of the hindering effect of multilayer graphene; crack deflection and crack branching occur and increase the fracture strength [33]. Accordingly, once debonding or separation occurs at the Al<sub>2</sub>O<sub>3</sub>/Cu interface to generate a microcrack, as shown in Fig. 11(b), the generated microcrack would propagate through Al<sub>2</sub>O<sub>3</sub> and Cu interfaces. When the microcrack extends and arrives at GNPs or C/Al<sub>2</sub>O<sub>3</sub> interface, as illustrated in Fig. 10(f), the embedded GNPs with large lateral dimension would hinder the crack path, or induce crack deflection or crack branching to dissipate more fracture energy. Therefore, the single-phase strengthening mechanisms of GNPs and Al<sub>2</sub>O<sub>3</sub> whiskers contribute to the improvement of mechanical properties when they uniformly disperse in the Cu matrix. Thus, the present study highlights the synergetic effects of the reinforcements on the mechanical properties of Cu-matrix composites: GNPs hinder the crack path generated at the Al<sub>2</sub>O<sub>3</sub>/Cu interface and enhance the already outstanding strengthening effect provided by Al<sub>2</sub>O<sub>3</sub> whiskers [26].

### **4 Conclusions**

- (1) The hardness of Al<sub>2</sub>O<sub>3</sub> whiskers and GNPs co-reinforced Cu-matrix composites ranges from HV 58.6 to 84.9, and their compressive strength ranges from 141.9 to 221.2 MPa. Both their hardness and compressive strength show a consistent tendency that firstly increases to a critical value in GNPs-0.5 composite and then decreases with increasing the amount of GNPs.
- (2) Grain refinement is a strengthening mechanism occurring during sintering due to an inhibition effect of grain growth by GNPs wrapping

or trapping. Besides, energy dissipating and load transfer are considered as the dominant strengthening mechanisms of both GNPs and  $Al_2O_3$  whiskers.

(3) The synergetic effect of Al<sub>2</sub>O<sub>3</sub> whiskers and GNPs is highlighted that the embedded GNPs would hinder the crack path generated at the Al<sub>2</sub>O<sub>3</sub>/Cu interface and enhance the already outstanding strengthening effect that Al<sub>2</sub>O<sub>3</sub> whiskers provide.

### **Acknowledgments**

The authors are grateful for the financial supports from the National Natural Science Foundation of China (No. 52101183), and China Postdoctoral Science Foundation (Nos. 2017M623054, 2018T110993).

#### References

- [1] YUE Hong-yan, YAO Long-hui, GAO Xin, ZHANG Shao-lin, GUO Er-jun, ZHANG Hong, LIN Xuan-yu, WANG Bao. Effect of ball-milling and graphene contents on the mechanical properties and fracture mechanisms of graphene nanosheets reinforced copper matrix composites [J]. Journal of Alloys and Compounds, 2017, 691: 755–762.
- [2] AKHTAR F, ASKARI S J, SHAH K A, DU X, GUO S. Microstructure, mechanical properties, electrical conductivity and wear behavior of high volume TiC reinforced Cu-matrix composites [J]. Materials Characterization, 2009, 60: 327–336.
- [3] ZHAO Zhan-yong, BAI Pei-kang, DU Wen-bo, LIU Bin, PAN Duo, DAS R, LIU Chun-tai, GUO Zhan-hu. An overview of graphene and its derivatives reinforced metal matrix composites: Preparation, properties and applications [J]. Carbon, 2020, 170: 302–326.
- [4] SHIN M K, LEE B, KIM S H, LEE J A, SPINKS G M, GAMBHIR S, WALLACE G G, KOZLOV M E, BAUGHMAN R H, KIM S J. Synergistic toughening of composite fibres by self-alignment of reduced graphene oxide and carbon nanotubes [J]. Nature Communications, 2012, 3: 19596–19600.
- [5] ZHAO Wen-min, BAO Rui, YI Jian-hong, HOU Xiang-hui, FANG Dong, LIU Chun-xuan. Fabrication of RGO/Cu composites based on electrostatic adsorption [J]. Transactions of Nonferrous Metals Society of China, 2020, 30: 982–991.
- [6] BANNARAVURI P K, BIRRU A K, DIXIT U S. Effect of laser surface melting on surface integrity of Al-4.5Cu composites reinforced with SiC and MoS<sub>2</sub> [J]. Transactions of Nonferrous Metals Society of China, 2020, 30: 344-362.
- [7] LONG Fei, GUO Xiu-hua, SONG Ke-xing, JIA Shu-guo, YAKUBOV V, LI Shao-lin, YANG Yu-bo, LIANG Shu-hua. Synergistic strengthening effect of carbon nanotubes (CNTs) and titanium diboride (TiB<sub>2</sub>) microparticles on mechanical

- properties of copper matrix composites [J]. Journal of Materials Research and Technology, 2020, 9: 7989–8000.
- [8] ZHANG Xin, LI Shu-feng, PAN Deng, KONDOH K. Microstructure and synergistic-strengthening efficiency of CNTs-SiC<sub>p</sub> dual-nano reinforcements in aluminum matrix composites [J]. Composites: Part A, 2018, 105: 87–96.
- [9] CHU Yan-hui, CHEN Peng-cheng, TANG Jing-da, RAO Ping-gen. Engineer in situ growth of α-Al<sub>2</sub>O<sub>3</sub> whiskers by axial screw dislocations [J]. Crystal Growth & Design, 2017, 17: 1999–2005.
- [10] WANG Yi-feng, CAO Jian, WANG Zhi-jie, CHEN Zhe, SONG Xiao-guo, FENG Ji-cai. Temperature-dependent transformation from whisker- to nanoparticle-strengthened composite interface in the Al<sub>2</sub>O<sub>3</sub>/Ag-based alloy system and mechanical properties of the joints [J]. Materials Characterization, 2015, 109: 50–56.
- [11] TAMURA Y, MOSHTAGHIOUN B M, GOMEZ-GARCIA D, RODRIGUEZ A D. Spark plasma sintering of fine-grained alumina ceramics reinforced with alumina whiskers [J]. Ceramics International, 2017, 43: 658–663.
- [12] IABAL A K M A, ARAI Y, ARAKI W. Effect of hybrid reinforcement on crack initiation and early propagation mechanisms in cast metal matrix composites during low cycle fatigue [J]. Materials & Design, 2013, 45: 241–252.
- [13] CORROCHANO J, CERECEDO C, VALCARCEL V, LIEBLICH M, GUITIAN F. Whiskers of Al<sub>2</sub>O<sub>3</sub> as reinforcement of a powder metallurgical 6061 aluminium matrix composite [J]. Materials Letters, 2008, 62: 103–105.
- [14] IQBAL A A, ARAL Y, ARAKI W. Fatigue crack growth mechanism in cast hybrid metal matrix composite reinforced with SiC particles and Al<sub>2</sub>O<sub>3</sub> whiskers [J]. Transactions of Nonferrous Metals Society of China, 2014, 24: 1–13.
- [15] NASEER A, AHMAD F, ASLAM M, GUAN B H, HARUN W S W, MUHAMAD N, RAZA M R, GERMAN R M. A review of processing techniques for graphene-reinforced metal matrix composites [J]. Materials and Manufacturing Processes, 2019, 34: 957–985.
- [16] RAMANATHAN T, ABDALA A A, STANKOVICH S, DIKIN D A, HERRERA-ALONSO M, PINER R D, ADAMSON D H, SCHNIEPP H C, CHEN X, RUOFF R S, NGUYEN S T, AKSAY I A, PRUD'HOMME R K, BRINSON L C. Functionalized graphene sheets for polymer nanocomposites [J]. Nature Nanotechnology, 2008, 6: 327–331.
- [17] WALKER L S, MAROTTO V R, RAFIEE M A, KORATKAR N, CORRAL E L. Toughening in graphene ceramic composites [J]. ACS Nano, 2011, 5: 3182–3190.
- [18] EIVANI A R, SHOJAEI A, PARK N, JAFARIAN H R. Fabrication of Cu-CuG nanocomposites with enhanced mechanical strength and reduced electrical resistivity [J]. Journal of Materials Research and Technology, 2021, 11: 650-666.
- [19] SUN Jia-lin, ZHAO Jun, CHEN Meng-jie, ZHOU Yong-hui, NI Xiu-ying, LI Zuo-li, GONG Feng. Multilayer graphene reinforced functionally graded tungsten carbide nanocomposites [J]. Materials & Design, 2017, 134: 171–180.
- [20] NIETO A, BISHT A, LAHIRI D, ZHANG C, AGARWAL A.

- Graphene reinforced metal and ceramic matrix composites: A review [J]. International Materials Reviews, 2017, 62: 241–302.
- [21] MOGHADAM A D, OMRANI E, MENEZES P L, ROHATGI P K. Mechanical and tribological properties of self-lubricating metal matrix nanocomposites reinforced by carbon nanotubes (CNTs) and grapheme—A review [J]. Composites Part B, 2015, 77: 402–420.
- [22] GÜLER Ö, BAGCI N. A short review on mechanical properties of graphene reinforced metal matrix composites [J]. Journal of Materials Research and Technology, 2020, 9: 6808-6833.
- [23] ATKINSON H V, DAVIES S. Fundamental aspects of hot isostatic pressing: An overview [J]. Metallur Mater Trans A, 2000, 31: 2981–3000.
- [24] BOCANEGRA-BERNAL M H. Hot isostatic pressing (HIP) technology and its applications to metals and ceramics [J]. J Mater Sci, 2004, 39: 6399–6420.
- [25] NIETO A, HUANG L, HAN Y H, SCHOENUNG J M. Sintering behavior of spark plasma sintered alumina with graphene nanoplatelet reinforcement [J]. Ceramic International, 2015, 41: 5926–5936.
- [26] GRIGORIEV S, PERETYAGIN P, SMIRNOV A, SOLI W, DIAZ L A, FERNANDEZ A, TORRECILLAS R. Effect of graphene addition on the mechanical and electrical properties of Al<sub>2</sub>O<sub>3</sub>–SiC<sub>w</sub> ceramics [J]. Journal of the European Ceramic Society, 2017, 37: 2473–2479.
- [27] CHEN B, SHEN J, YE X, IMAI H, UMEDA J, TAKAHASHI M, KONDOH K. Solid-state interfacial reaction and load transfer efficiency in carbon nanotubes (CNTs)-reinforced aluminum matrix composites [J]. Carbon, 2017, 114: 198–208.
- [28] KIM W J, LEE T J, HAN S H. Multi-layer graphene/copper composites: Preparation using high-ratio differential speed rolling, microstructure and mechanical properties [J]. Carbon, 2014, 69: 55–65.
- [29] CHEN Z Z, TOKAJI K. Effects of particle size on fatigue crack initiation and small crack growth in SiC-particulate reinforced aluminium matrix composites [J]. Materials Letter, 2004, 58: 2314–2321.
- [30] GUO Q, KONDOH K, HAN S M. Nanocarbon-reinforced metal-matrix composites for structural applications [J]. MRS Bulletin, 2019, 11: 40–45.
- [31] KIM Y, LEE J, YEOM M S, SHIN J W, KIM H, CUI Y, KYSAR J W, HONE J, JUNG Y, JEON S, HAN S M. Strengthening effect of single-atomic-layer graphene in metal–graphene nanolayered composites [J]. Nature Communications, 2013, 4: 2114.
- [32] HWANG B, KIM W, KIM J, LEE S, LIM S, KIM S, OH S H, RYU S, HAN S M. Role of Graphene in reducing fatigue damage in Cu/Gr nanolayered composite [J]. Nano Letter, 2017, 17: 4740–4745.
- [33] LI Zuo-li, ZHAO Jun, SUN Jia-lin, GONG Feng, NI Xiu-ying. Reinforcement of Al<sub>2</sub>O<sub>3</sub>/TiC ceramic tool material by multi-layer graphene [J]. Ceramics International, 2017, 43: 11421–11427.

### Al<sub>2</sub>O<sub>3</sub> 晶须与石墨烯纳米片共增强铜基复合材料的 显微结构及界面行为

邵甄胰 1,2. 潘恒康 2. 舒 锐 3. 蒋小松 1. 朱旻昊 1

- 1. 西南交通大学 材料科学与工程学院,成都 610031;
- 2. 成都工业学院 材料与环境工程学院,成都 611730;
- Forschungszentrum Jülich GmbH, Institut für Energie-und Klimaforschung-Plasmaphysik,
  52425 Jülich, Germany

摘 要: 研究 Al<sub>2</sub>O<sub>3</sub> 晶须和石墨烯纳米片共增强铜基复合材料的力学性能和显微结构。采用机械合金化、真空热压烧结和热等静压工艺制备不同石墨烯含量的铜基复合材料。含 0.5%石墨烯(质量分数)的铜基复合材料(GNP-0.5) 具有良好的 Cu/C 和 Cu/Al<sub>2</sub>O<sub>3</sub> 界面结合性能;复合材料的硬度和抗压强度随石墨烯含量的增加呈现先增加到一个临界值后减小的趋势。研究结果表明,石墨烯和 Al<sub>2</sub>O<sub>3</sub> 晶须在铜基复合材料中最主要的强化机制是能量耗散和载荷传递以及石墨烯导致的晶粒细化。石墨烯与 Al<sub>2</sub>O<sub>3</sub> 晶须的双相混杂增强效应在于:当 Al<sub>2</sub>O<sub>3</sub>/Cu 界面存在微裂纹并沿着界面扩展时,嵌于铜基复合材料中的石墨烯会阻碍裂纹扩展路径,从而强化 Al<sub>2</sub>O<sub>3</sub> 晶须在铜基复合材料中的增强作用。

关键词: 石墨烯; Al<sub>2</sub>O<sub>3</sub> 晶须; 铜基复合材料; 显微结构; 界面行为

(Edited by Bing YANG)